SYNTHESIS, STRUCTURE AND CATALYTIC PROPERTIES OF MONO - AND BIMETAL - OXIDE Pt / γ - Al_2O_3, Au / γ - Al_2O, Au - Pt / γ-Al_2O_3 AND Pt – Au/ γ-Al_2O_3 NANOCOMPOSITES OBTAINED BY FLUID - AND METAL - VAPOR METHODS

Ernest Said-Galiev[1], Alexander Nikolaev[1], Sergei Abramchuk[1], Alexei Khokhlov[1], Alexander Vasilkov[1], Andrew Lisitsyn [1], Alexander Naumkin[1], Ilya Volkov[1], Olga Lependina[1], Eleonora Shtykova[2], Cyril Dembo[2], Can Erkey[3]

[1]State Institution of Russian Academy of Sciences A.N. Nesmeyanov Institute of Organoelement Compounds RAS, Vavilova Str., 28, Moscow 119991, Russia
[2]State Institution of Russian Academy of Sciences A.V. Shubnikov Institute of Crystallography RAS, Lenin prosp. 59, Moscow 1193331, Russia
[3]Dep. of Chem. and Biolog. Engineering., Koc Univ., 34450 Sariyer, Istanbul, Turkey
ernest@ineos.ac.ru; *Fax: +7(499)1355085*

Bimetallic nanocomposites have been synthesized with a help of supercritical carbon dioxide (SC CO_2) (fluidic method) and metal-vapor synthesis (MVS) and bimetallic composites of noble metals Pt and Au and γ-Al_2O_3 matrix have been made by combination of these two methods. The synthesis technique has been developed and the structure, concentration and chemical state of a metal in the composites has been investigated by SAXS, TEM, X-ray FA and ESHA methods. Neural state of metal atoms in clusters is shown and their size distribution in the range of 1-50 nm dictated as it turned out with pore sizes of rigid matrices was found by SAXS.

The composites obtained have shown excellent catalytic properties in the reaction full oxidation of CO in to CO_2.

Key words: fluidic method, metal-vapor synthesis, metal-oxide nanocomposite, bimetallic nanocomposite, SAXS, ESCA, TEM, X-ray FA, Pt / γ-Al_2O_3 , Au / γ-Al_2O_3 , Au - Pt / γ-Al_2O_3.

Bimetallic catalytic systems pay last years much attention of researchers because they possess to manipulate with their activity and selectivity relation by selecting of a metals pair. These pairs are chosen in this way that first metal would provide an activity and second one would answer for influence selectivity. Such properties especially effectively become apparent in alloys but bimetallic catalysts of "core-shell" structure as turned out are more effective else [1-5].

Last years some articles were published in which SC CO_2 was used as a solvent and a medium for reduction of catalysts metals. The investigations on synthesis in SC CO_2 medium of Pt/carbonic material catalyst for fuel cell [6-16] and some heterogeneous catalysts [17, 18] are known. An activity and a selectivity of these catalysts by the author s data exceed in subsequent properties of catalysts obtained in organic solvents media.

The use of supercritical fluids (SCF) for the synthesis and processing of nanomaterials has gained considerable interest in recent years. SCF exhibits an attractive combination of the solvent properties of a gas and a liquid.

It can dissolve solutes such as a liquid and yet possess low viscosity, high diffusivity, and zero surface extension like a gas. Furthermore, the solvent strength of SCF can be varied by manipulating fluid temperature and pressure, thus allowing a degree of control and rapid separation of products, which is impossible using conventional solvents. It provides a rapid, direct, and clean approach to preparing nanomaterials and nanocomposites. These special and unique features make SCF an attractive medium for delivering reactant molecules to areas with high aspect ratios, complicated surfaces, and poorly wettable supports. Supercritical carbon dioxide (SC CO_2) allows reactive components to penetrate inside the porous materials themselves, partitioning into the inner regions of the porous supports [19]. Considerable advantage of SC CO_2 is its ecological purity, because it is included in atmosphere composition. It does not demand of mandatory recuperation. Its maximum concentration in atmosphere is equal to 5%, while for acetone 7.5 10^{-3} %, pentane 6 $\cdot 10^{-3}$ %, chloroform $0.01 \cdot 10^{-3}$ % [20].

The paper is devoted to synthesis and structure investigations of mono- and bi nano metal-oxide composites Pt / γ-Al_2O_3, Au / γ-Al_2O_3, Au-Pt / γ-Al_2O_3 and Pt- Au/ γ-Al_2O_3 , obtained with a help of SC CO_2 and MVS. The last provides in combination with SC CO_2 more technological versatility. The structure of obtained composites was studied with X-ray EA, XD, TEM, ESCA and SAXS. All synthesized structures have shown effective catalytic properties in the reaction of CO in to CO_2 full oxidation.

Materials and methods

Materials: γ-Al_2O_3 (IKT-02-6 M from "\Katalysator", Novosibirsk, S_{sp} = 138 m^2 g^{-1}). The support was activated at 300 ^oC for 3 hours, after that it was saved in argon. SC CO_2 of 99, 997 vol. %, and high purity hydrogen were used. The metal precursor for SC technology (1, 5-cyclooctadiene)dimethylplatinum (II) COD $Pt(CH_3)_2$ (Pt content = 58.7 %), temperature of decomposition is 150-200 ºC, (received from "Aldrich" and used without additional purification). This complex was selected due its enough solubility in SC CO_2 (more than 14.6 mg cm^{-3} at 80 ºC and 27.6 MPa) [14]. Gold (99, 99%) as a foil and triethylamine (98%) (Aldrich). Triethylamine was dried and distilled under Na in argon atmosphere.

The sets*:* the *sets* were described elsewhere [21, 22].

Methods of synthesis

Synthesis of metal nanocomposites:

Synthesis in fluid medium: the load of γ-Al_2O_3 support (1-1,5g) and metal precursor colorless crystalline COD Pt $(CH_3)_2$ (1 % from support mass) are introduced into reactor with inside volume of 5 cm^3 and stir-bar with Teflon covering. Reactor is sealed, purged with pure CO_2 flow and heated up to 100-120 ^oC in silicone bath mounted on heating magnetic stirrer "RCT basic" IKA WERKE. The pressure 20-25 MPa is generated with syringe press, and the reaction system is sustained at a mixing for 4 – 6 hours. Then the reactor is cooled and depressurized. A metal reduction is carry out in dry argon flow (10-20 cm^3 / min at 200^o C for 6 hours). Then the reactor is cooled, depressurized and then the support immobilized with metal particles is washed using Shot's filter number 3 some times with Et OH for removal of unreduced complex and its decomposition products. The composite is dried finally in vacuum at 80 ^oC for 2 hours.

MVS is carried out on the methodic of stable colloid metals making by common condensation of gold vapors with triethylamine at – 196 – 193 ^oC developed by the authors earlier. An

immobilization of nanoclusters on the support is carried out after melting of the condensate [17, 18]. Bimetal catalysts were synthesized by successive immobilization of metals on the support by combination of fluid and MVS techniques.

Analytical methods

Small angle X-ray scattering (SAXS):

SAXS was carried out by method of traditional SAXS on modified laboratory diffractometer AMUR-K (development of Institute of Crystallography of Russian Academy of Sciences) on fixed wave length of irradiation λ = 0.1542 nm with application of Cratky´s geometry [23, 24]. Modification of the device and use of detector with improved parameters lets to use more wide area of wave vectors in the range $0.12 < s > 7$ nm^{-1} ($s = 4\pi \sin \Theta/\lambda$, *2 Θ- scattering angle*). Interactive program GNOM [24] was used for analysis of platinum nanoparticle size distribution. In this case a volume function of size distribution $D_v(R)$ was found on integral equation:

$$I(s)=(\Delta\rho)^2 \int_{R_{min}}^{R_{max}} D_V(R) m^2(R) i_0(sR) dR \qquad (1)$$

in assumption of scattering objects sphericity. Here $I(s)$ – intensity of scattering, R – sphere radius, R_{min} and R_{max} minimal and maximum sizes, $i_0(x)=\{[\sin(x) - x\cos(x)] / x^3\}^2$ and $m(R)= (4\pi/3)R^3$ - accordingly sphere form-factor and its volume. In the calculations R_{min} was assumed to be equal 0 and R_{max} and selected individually for every specific case taking into account maximal coincidence of the model and experimental curves of small angle scattering. The distances distribution function $p(r)=r^2\gamma(r)$ was calculated on experimental data with GNOM program of inverse indirect Fourier transform [25], using the relation

$$\gamma(r) \approx \frac{1}{2\pi^2} \int_{s=0}^{S_{max}} s^2 I(s) \cdot \frac{\sin(sr)}{sr} ds \qquad (2)$$

The $p(r)$ function was used also for determination of maximal sizes of scattering objects D_{max}.

X-ray fluorescent analysis: Platinum concentration was determined with X-ray fluorescent analyzer VRA 30 (Germany) using Pt $L_{\alpha 1}$ line. Determination of platinum mass and concentration in experimental samples is based on the spectra of reference samples. All the samples were produced by method [26].

X-ray photoelectron spectroscopy: The XPS or ESCA spectra were recorded on a Kratos XSAM-800 spectrometer using Mg Kα radiation (90 W) at about 10^{-8} Torr. The XPS spectra were background subtracted (assuming linear and Shirley background due to the secondary electrons for the insulating catalysts and metal foils, respectively) and fitted with Gaussian line profiles. The quantitative analysis was based on the atomic sensitivity factors. Photoelectron spectra were measured with interval of 0.1 eV. The energy scale of the spectrometer was calibrated using next values of binding energy: Cu $2p_{3/2}$ – 932.7 eV, Ag $3d_{5/2}$ – 368.3 eV, Au $4f_{7/2}$ – 84.0 eV [27]. The surface charging of the support spectra was done using the C1s spectrum by routine method. A calibration of Pt / γ - Al_2O_3 spectra was carried out using the Al2p peak of the support spectrum.

RESULTS

The data on structure of the catalyst obtained with SAXS are presented below.

An analysis of small-angle scattering curves of Pt / γ- Al_2O_3 composite for the initial matrix, matrix impregnated with complex COD Pt(CH_3) and the matrix with reduced Pt nanoparticles (these curves are not presented) show that initial matrix and matrix impregnated with the complex do not practically differ on small angle scattering as a difference in electron density of the matrix and impregnated complex is very small. This is connected also with low complex concentration (~0.6 %).

After platinum reduction and formation of nanoparticles increase of scattering amplitude is clear detected, that indicates to successive reduction of the metal. After subtraction of support scattering from scattering of the sample with reduced Pt, the difference curve was obtained. The curve that reflects only Pt nanoparticles scattering was used for calculation of size distribution of metal nanoparticles. Pore size in aluminum support was calculated with scattering curve of initial matrix. All obtained size distributions are presented in Fig.1.

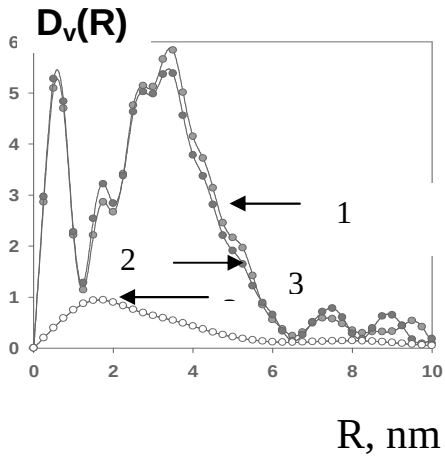

Fig. 1. Size distribution of the scattering heterogeneities of the original matrix and Pt-containing samples: 1- pristine γ-Al_2O_3 support, 2- the support impregnated with a complex of COD Pt $(CH_3)_2$, 3- the support with reduced complex.

The pore size distribution is bimodal (d = 1 nm and 6.5 nm). The shape of curves 1 and 2 is the same, so the contribution of COD Pt $(CH_3)_2$ is negligible. Reduced particles have a wide distribution profile with a maximum of ~ 1.5 nm (d = 3-3.5 nm) and a number of larger particles. The distribution amplitude is much smaller than that of the $D_v(R)$ function of the matrix because of the low concentration (0.34%) of nanoparticles in the sample. Data of analysis of Pt /γ-Al_2O_3 metal-composite by TEM are presented in Fig. 2

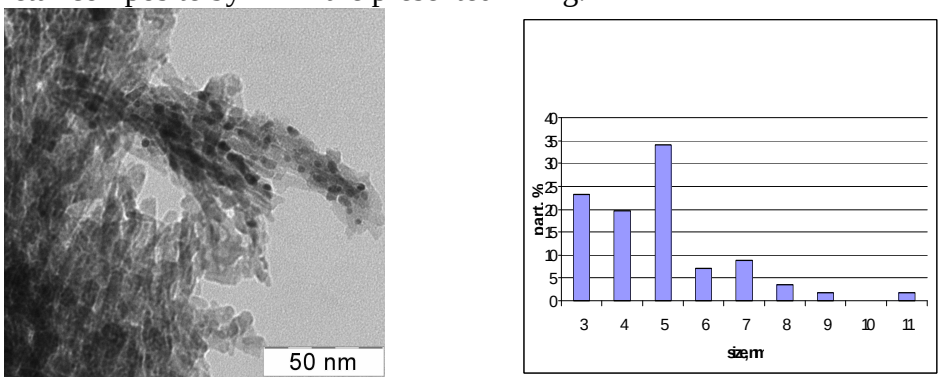

Fig. 2. TEM micrograph of Pt / γ -Al_2O_3 and size distribution histogram of Pt particles (electron microscope "Leo 912 AB-OMEGA" of "Sarl Zeiss" brand, an accelerating voltage of 80 kV. Platinum-impregnated samples of aluminum oxide grains were placed in epoxy resin. Sections were obtained from microtome "Reichert-jung" in steps of 50 nm). Sections were obtained from microtome "Reichert-jung" in increments of 50 nm). Medium particle size calculated is Pt = 4.87 ± 1.08 nm (average standard deviation), selection 56.

Chemical state of metal atoms on the surface of monometallic catalyst Pt / γ-Al_2O_3 was investigated by ESCA. The same peaks were present both in synoptic spectrum of the catalyst and in the support spectrum.

Pt 4f peaks are not found in the survey spectrum because of low Pt concentration evident and overlapping with Al 2p peak. In high resolution spectrum one can discriminate between the Pt 4f and Al peaks using the spectrum decomposition based on a reference Al 2p spectrum of the support. A shoulder in the region of low binding energy is caused with presence of the Pt $4f_{7/2}$ peak. The Pt 4f spectrum obtained as difference between the catalyst and support spectra is shown in Fig. 3.

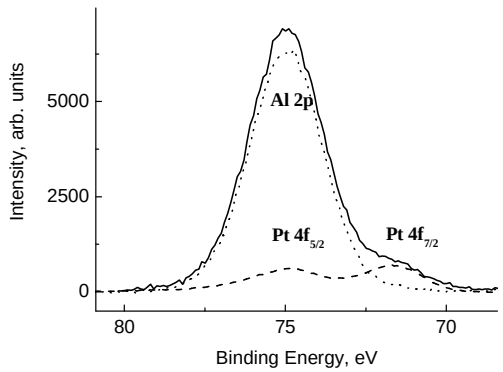

Fig.3. The selection of the spectrum Pt4f of catalyst Pt / γ-Al_2O_3.

Binding energies of the peaks Pt $4f_{5/2}$ and Pt $4f_{7/2}$ are 74.9 and 71.6 eV, respectively, and they are fingerprints of a metal state.

The Al 2p photoelectron spectrum of the support can be described with one state binding energy of which corresponds to reference data Al_2O_3 [27, 28].

The structure of Pt - Au / γ- Al_2O_3 bimetallic catalyst was also investigated by SAXS. The experimental curves of SAXS have ill-defined Bragg′s maximums at s = 0.8 nm^{-}. Since these reflexes are noticed on all scattering curves and locate at the same place it can be concluded that porous aluminum matrix does not change its structure after inclusion of metal particles into it. This allows to subtract a matrix scattering from overall one of the samples and to obtain difference curves reflecting only nanoparticles scattering. These curves were used for calculation of nanoparticles size distribution, which are incorporated into porous aluminum oxide. These volumetric size distribution functions are shown on Fig.4.

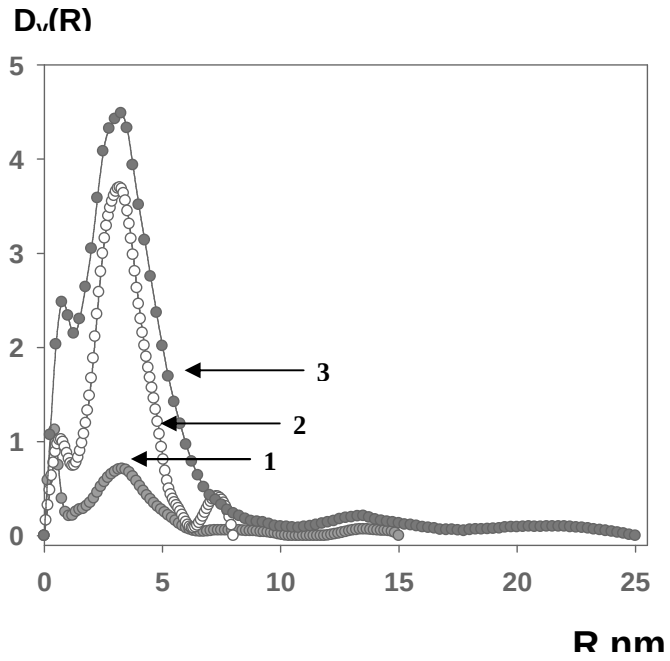

Fig.4. Volumetric size distribution function for pores of aluminum matrix (1), Au nanoparticles (2) and the combined Au and Pt nanoparticles (3), calculated using GNOM program [24].

It is evident that the curves of the function $D_V(R)$ are rather similar, so metal nanoparticles are formed in the pores of the matrix and governed with its shape.

The main fraction are nanoparticles with R = 3 nm. There are also small particles with radius about 0.3-0.4 nm and a small number of large

nanoparticles with a radius of 25 nm. The narrowest size distribution of nanoparticles corresponds to gold and the most widespread – to combined nanoparticles.

Nanoparticle sizes in granules calculated by independent method with MIXTURE program have confirmed the results obtained with GNOM one: the sample contains 64 % of nanoparticles with a radius of 3.5 nm and 32% with a radius of about 10-15 nm. Nanoparticles of diffrent sizes (about 4 %) are also present.

The SAXS curve of the γ-Al_2O_3 support is characterized by presence of central scattering related to presence of structural inhomogeneities and with a small maximum in the area of 1 nm^{-1}. The maximum can be an indicator of a scattering object shape in granules. Filled or free pores are available to play role of such objects. We have taken a shot to determine the form of these scattering inhomogeneities in granules.

Fig. 5. The distribution function over distances *p(r),* calculated using GNOM program and "average shape of the scattering objects in a granule γ-Al_2O_3 (shown in the box above right), recovered by DAMMIN program.

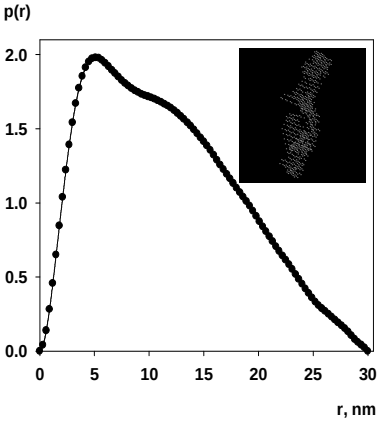

The shape of the pair function (distribution function over distances) is characteristic for elongated bodies such as cylinder. Reconstructed averaged shape is really close to cylindrical as well. The length of the cylinder is about 30 nm and a cross section is about 6 - 7 nm.

The main fraction of scattering metal nanoparticles in the support granules are objects with a size of 6-7 nm (radius about 3 - 4 nm) that coincides with cross-section of conditional cylinder of reestablished form. Smaller nanoparticles with size of about 1 nm are also present. Maximal size of scattering pores in granules (30 nm) is also coincides with a presence in the sample of metal nanoparticles with size of 20-30 nm. Based on obtained data, it is possible to propose a next structural model of scattering objects in granules: presumably cylindrical pores in granules with a length of about 30 nm filled with nanoparticle clusters with a size of about 6 nm composed from smaller nanoparticles. Chemical state of metal atoms of bimetallic catalyst was investigated by ESCA.

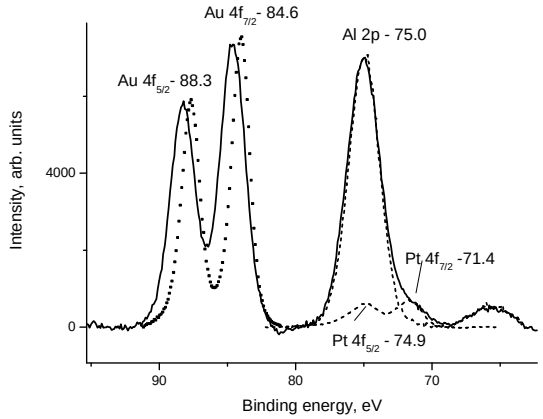

Fig. 6. Photoelectron spectrum of the catalyst in the region of Au 4f, Pt 4f and Al 2p peaks.

Binding energy of $4f_{7/2}$, Au $4f_{5/2}$, Pt $4f_{7/2}$ и Pt $4f_{5/2}$ peaks, equal to 84.6, 88.3, 71.4 and 74.9 eV, respectively, are characteristic for metallic particles. The Au 4f peaks shift toward higher binding energy by 0.6 eV is not indicative of the formation of surface Au-Pt alloy, because the shift would have the opposite direction because of the higher electronegativity of Au atom in comparison with that of Pt [29]. However, the Au 4f spectrum can be

represented as the sum of the two states, one of which is related to the interaction between Au and Pt while other to that between Au and oxygen atoms of the support.

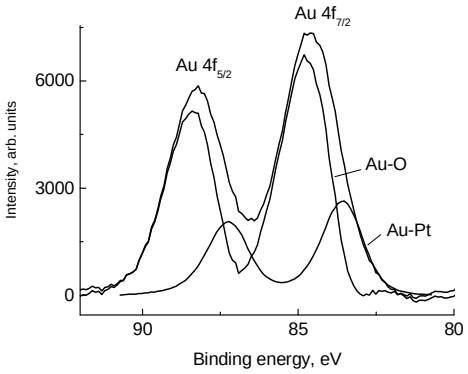

Fig. 7. Decomposition of the Pt 4f spectrum of Au-Pt / γ -Al_2O_3 on the components: Au-Pt and Au-O (Al_2O_3).

Using the value of the chemical shift for the Au 4f $_{7/2}$ peak for the Pt-Au / C system, (equal to -0.38 eV) we presented Au 4f spectrum as a sum of two states, one of which corresponds to the Au – Pt system, and the other to Au-O-Al. The relative intensity of the first state is 26%. The appearance of an additional state in the O 1s spectrum of the Au-Pt/ γ-Al_2O_3 catalyst, which is absent both in spectrum of the support and of the system Pt / γ -Al_2O_3, confirms this version.

Fig. 8. The dependence of catalytic conversion CO into CO_2 on temperature for the *Pt / Al_2O_3* sample**.**

Composition of reaction mixture: CO - 2%, O_2 - 4%, in the atmosphere of He. Chromatograph "Crystal 2000m", software "Chromatec Analyst 2.5" in the temperature range 20 - 400 º C at atmospheric pressure, volumetric flow rate of gases 1 ml / sec.

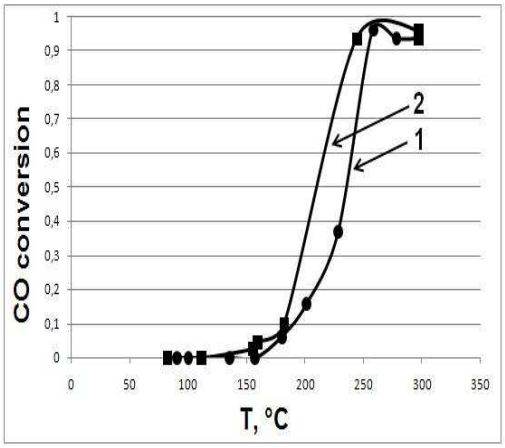

Lead-up of the sample in a stream of CO + O_2 + He + H_2 for 10 min. The heating was carried out on 20 °C from room temperature (without heating) to a temperature of 394 °C. Recording was begun at 78 °C (curve 1). Then the cycle was carried out in the opposite direction by 50 °C from 333 °C to 91 °C (curve 2). The sample showed no activity up to 200 °C; at 300 °C conversion reached 100%. On the reverse cycle 13% conversion was observed at 200 °C.

Fig.9. *Au/ γ-Al_2O_3* (MVS).

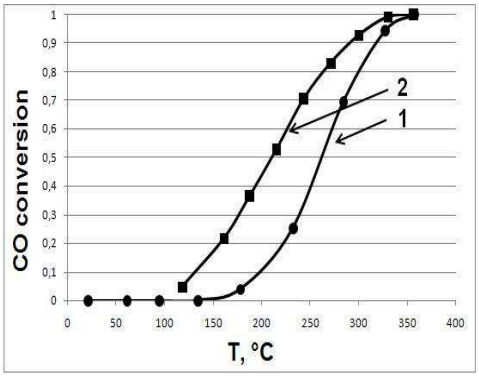

Composition of reaction mixture: CO - 2%, O_2 - 4%, in the atmosphere of He . Chromatograph "Crystal 2000m", software "Chromatec Analyst 2.5" in the temperature range 20 - 400 º C at atmospheric pressure, volumetric flow rate of gases 1 ml / sec. The sample showed no activity up to 200 °C; at 350 °C conversion reached 100% (curve 1). On the reverse cycle 45% conversion was observed at 200 °C (curve 2). So 100% conversion for Au is noticed at higher temperature as compared with Pt.

Initial temperature of activation is approximately the same.

.

Fig . 10. ***Au-Pt/Al$_2$O$_3$*** (Au - MVS, Pt - SC CO_2).

Composition of reaction mixture: CO - 2%, O_2 - 4%, in the atmosphere of He.

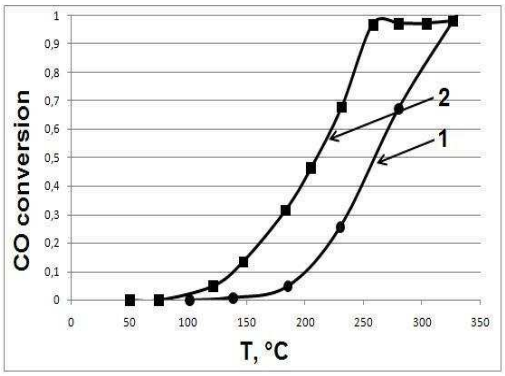

Lead-up of the sample in a stream of CO + O_2 + He + H_2 for 10 min. Composition of reaction mixture: CO - 2%, O_2 - 4%, in the atmosphere of He.

The heating was carried out by step of 40° C from room temperature to 330° C (curve 1). The sample showed no activity up to 180° C; at 330 °C conversion reached 100%.

On the reverse cycle 34 % the conversion was observed at 180 °C (curve 2).

Evidently, a strong activation has taken place.

The catalyst does not loose of activity at repeated cycles.

Fig. 11. *Pt /Au- /Al$_2$O$_3$* (Au - MVS, Pt – SC CO_2).

Lead-up of the sample in a stream of CO + O_2 + He + H_2 for 10 min.

The heating was carried out by 50 °C step from room temperature (without heating) to 330 °C (curve 1).

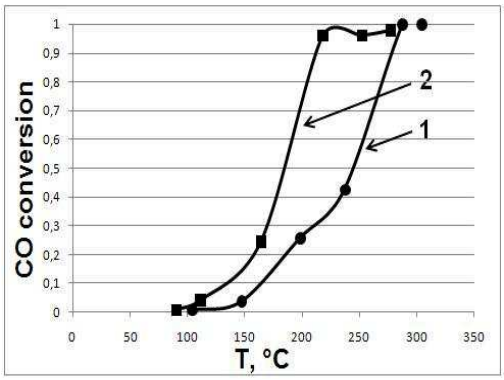

Then the cycle was carried out in the opposite direction by 25 °C step from 330 °C to 50 °C (curve 2).

The sample showed no activity up to 160 °C; at 300 °C conversion reached 100 % on the reverse cycle 24 % conversion was observed at 160 °C.

Evidently, a strong activation has taken place, as well.

Thus, an addition of gold enhances the activity of Pt / γ-Al$_2$O$_3$.

The task for this reaction - to achieve activation of the catalyst at room temperature (application as protective masks at fires).

CONCLUSION

1. Fluid and MVS procedures of noble metal nanoparticles immobilization on γ-Al_2O_3 support have been developed and the metal nanocomposites of gold (MVS) and platinum (SC CO_2) have been synthesized
2. Bimetallic metal-oxide nanocomposites of gold and platinum with γ-Al_2O_3 have been prepared by combination of these procedures.

3. The structure, concentration and chemical state of metal atoms in the composites have been investigated by SAXS, TEM, ESCA и X-ray FA methods and a structural model of the bimetallic catalyst granule has been proposed

4. Metal nanoparticles formed in γ-Al_2O_3 matrix are of neutral state and have a size in the ranges of 1-50 nm with size distribution profile coincident with one of rigid matrix pores

5. Both synthesized mono- and bimetal-oxide composites of Pt and Au with γ-Al_2O_3 have shown a good catalytic activity in the reaction full oxidation of CO into CO_2. Addition of Au to Pt / γ-Al_2O_3 system increases catalytical activity of the latter.

ACKNOWLEDGEMENTS

The authors would like to thank The Russian Fond of Basic Research (grant RFBR 11-03-01062-a), Russian Academy of Sciences (Programs OCH-6, OCH-7, OCH-2 and P-21) and Ministry of Education and Science (State contract FAE P-924) for financial support.

REFERENES:

[1] DHEPE, P., FUKUOKA,A., ICHIKAWA, M., Phys. Chem. Chem. Phys. Vol. 5, **2003,** p. 5565

[2] JUN-SONG, Y., QIAN-WANG, CH., CHINESE JOURNAL OF CHEMICAL PHYSICS. Vol. 21, **2008**. N 1, p. 76.

[3] KAMEO, A., TOMOKAZU, Y., KUNIO E., Colloids and Surfaces A: Physicochem. Eng. Aspects. Vol. 215, **2003, p**. 181

[4] YEN CLIVE H., SHIMIZU, KENICHI, LIN YING-YING et al., Energy & Fuels, Vol. 21, **2007**, p. 2268

[5] LIN, YUEHE, XIAOLI, CUI, YEN, ClIVE H. et al., Langmuir, Vol. 21, **2005,** p. 11474

[6] BAYRAKÇEKEN, A., CANGÜL, B., ZHANG, L.C. et al., Int. J. Hydrogen. Energy. Vol. 35, **2010,** p. 11669

[7] CANGÜL, B, ZHANG, L.C., AINDOW, M. et al. , J. Supercrit. Fluids. **2009.** V. 50. P. 82.

[8] BAYRAKÇEKEN, A., SMIRNOVA, A., KITKAMTHORN, U. et al., Chem. Eng. Comm. Vol. 196, **2009.** p. 1

[9] ZHANG, Y., CANGUL, B, GARRABOS, Y. et al., J. Supercrit. Fluids, Vol. 44, **2008,** p. 7

[10] ERKEY, C., J. Supercrit. Fluids, Vol. 47, **2009,** p. 517

[11] ZHANG, Y., CANGUL, B., GARRABOS, Y. et.al., J. Supercrit. Fluids, Vol. 44, **2008,** p. 71

[12] BAYRAKÇEKEN A., SMIRNOVA, A., KITKAMTHORN, U. et al., Journal of Power Sources. V. 179, **2008**, p. 532

[13] BAYRAKCEKEN, A., KITKAMTHORN, U., AINDOW, M. et al., Scripta Materialia, Vol. 56, **2007,** p.101

[14] ZHANG, Y., ERKEY, C., J. Supercrit. Fluids, **2006,** p. 252

[15] JANG, R., ZHANG, Y., SWIER, S., Electrochemical and Solid State Letters, Vol. 8, **2005,** p. A 611

[16] ZHANG, Y., KANG, D., SAQUING, C., et al., Ind. Eng. Chem. Res., Vol. 44, **2005,** p. 4161

[17] SOLODOVNIKOV, S., VASIĽKOV, A., OLENIN, A., et al., Докл. АН СССР, **1990.** Vol. 310, № 4, p. 912

[18] VASIL'KOV, A., OLENIN, A., TITOVA, E. et al., J. Colloid Interface Sci., Vol. 169, **995.** p. 356
[19] YUEHE, LIN, XIAOLI, CUI, ClIVE, H., YEN at al., *Langmuir*, Vol. 21 (24), **2005**, p. 11474

[20] BECKMAN, E., J. of Supercrit. Fluids, Vol. 28, **2004,** p. 121
[21] SAID-GALIEV, E., GAMZAZADE, A., GRIGOR'EV, T. et al., NANOTECHNOLOGIES IN RUSSIA, Vol. 6, **2011**, Nos. 5–6, p. 341

[22] SERGEEV, V., VASIĽKOV, A., LISICHKIN, G., Russian chemical Journal, Vol. XXXII, **1987,** p. 96

[23] MOGILEVSKII, L., DEMBO, A., SWERGUN, D., Feigin, L., Cristallography, Vol. 29, **1984**. No. 3, p. 587
[24] FEIGIN, L., SVERGUN, D., Structure Analysis by Small-Angle X-ray and Neutron Scattering, N-Y., Plenum Press, **1987**, 350 c
[25] SVERGUN, D., Biophys. J., Vol.76 (6), **1999,** p. 2879; J. Appl. Cryst., Vol. 25, **1992,** p. 495
[26] GELMAN, N., TERENŤEVA, E., SHANINA , T., Methods of quantitative organoelement microanalysis, M., Chemistry, **1987**, p. 240
[27] Wagner, C., Riggs, W., Davis, L. et al., Handbook of X-ray Photoelectron Spectroscopy, G. Muilenberg (ed), MN., Perkin-Elmer, **1979**
[28] Wagner, C., Naumkin, A., Kraut-Vass, A. et al., NIST X-ray Photoelectron Spectroscopy Database, Version 3.5 (National Institute of Standards and Technology, Gaithersburg, **2003**); http://srdata.nist.gov/xps/
[29] Selvarani, G., Selvaganesh, S. V., Krishnamurthy, S.G. V. et.al., J. Phys. Chem. *C*, Vol. 113**, 2009**, p. 7461.